Biomaterials 101 (2016) 241–250

Contents lists available at ScienceDirect

Biomaterials

journal homepage: www.elsevier.com/locate/biomaterials

Localized sequence-specific release of a chemopreventive agent and an anticancer drug in a time-controllable manner to enhance therapeutic efficacy

Wen-Yu Pan [a, 1], Kun-Ju Lin [b, c, 1], Chieh-Cheng Huang [a, 1], Wei-Lun Chiang [a], Yu-Jung Lin [a], Wei-Chih Lin [a], Er-Yuan Chuang [a], Yen Chang [d, e, **], Hsing-Wen Sung [a, *]

[a] Department of Chemical Engineering and Institute of Biomedical Engineering, National Tsing Hua University, Hsinchu, Taiwan, ROC
[b] Department of Medical Imaging and Radiological Sciences, Chang Gung University, Taoyuan, Taiwan, ROC
[c] Department of Nuclear Medicine and Molecular Imaging Center, Chang Gung Memorial Hospital at Linkou, Taoyuan, Taiwan, ROC
[d] Department of Cardiovascular Surgery, Heart Center, Cheng Hsin General Hospital, Taipei, Taiwan, ROC
[e] Collage of Medicine, National Yang Ming University, Taipei, Taiwan, ROC

ARTICLE INFO

Article history:
Received 7 April 2016
Received in revised form
30 May 2016
Accepted 2 June 2016
Available online 4 June 2016

Keywords:
Sequential drug release
Combination chemotherapy
Reactive oxygen species
Chemopreventive agent
Synergistic anticancer effect

ABSTRACT

Combination chemotherapy with multiple drugs commonly requires several injections on various schedules, and the probability that the drug molecules reach the diseased tissues at the proper time and effective therapeutic concentrations is very low. This work elucidates an injectable co-delivery system that is based on cationic liposomes that are adsorbed on anionic hollow microspheres (Lipos-HMs) *via* electrostatic interaction, from which the localized sequence-specific release of a chemopreventive agent ($1,25(OH)_2D_3$) and an anticancer drug (doxorubicin; DOX) can be thermally driven in a time-controllable manner by an externally applied high-frequency magnetic field (HFMF). Lipos-HMs can greatly promote the accumulation of reactive oxygen species (ROS) in tumor cells by reducing their cytoplasmic expression of an antioxidant enzyme (superoxide dismutase) by $1,25(OH)_2D_3$, increasing the susceptibility of cancer cells to the cytotoxic action of DOX. In nude mice that bear xenograft tumors, treatment with Lipos-HMs under exposure to HFMF effectively inhibits tumor growth and is the most effective therapeutic intervention among all the investigated. These empirical results demonstrate that the synergistic anticancer effects of sequential release of $1,25(OH)_2D_3$ and DOX from the Lipos-HMs may have potential for maximizing DOX cytotoxicity, supporting more effective cancer treatment.

1. Introduction

Doxorubicin (DOX) is an anticancer drug that has been extensively used to treat a variety of human tumors, including early and advanced breast cancers, by systemic administration [1–3]. However, systemically administered antitumor medication frequently results in rapid clearance of the drug from circulation and poor distribution to the target tissue [4]. Localized delivery of a carrier may concentrate the drug within the tumor, increasing therapeutic effectiveness and reducing systemic toxicity [5,6].

One of the proposed mechanisms of the cytotoxic effect of DOX on tumor cells involves its overproduction of reactive oxygen species (ROS) such as superoxide radicals, which exert irreversible oxidative damage to the cells [7]. The extent of this oxidative cellular damage is determined by the rate of intracellular ROS production and the efficiency of the defense mechanisms of the cells [8,9]. Superoxide dismutase (SOD), an antioxidant enzyme, actively participates in cellular defenses against oxidative damage that is caused by superoxide radicals [10]. Recent studies have suggested that the treatment of tumor cells with 1,25-dihydroxyvitamin D_3 ($1,25(OH)_2D_3$), a chemopreventive agent, markedly reduces the intracellular expression of SOD, significantly reducing the antioxidant capacity of the cells [11–13]. Therefore, reduction of the cellular expression of SOD by $1,25(OH)_2D_3$ has

* Corresponding author. Department of Chemical Engineering, National Tsing Hua University, Hsinchu 30013, Taiwan, ROC.
** Corresponding author. Department of Cardiovascular Surgery, Heart Center, Cheng Hsin General Hospital, Taipei, Taiwan, ROC.
E-mail addresses: cvsyenchang@gmail.com (Y. Chang), hwsung@mx.nthu.edu.tw (H.-W. Sung).
[1] The first three authors (W.Y. Pan, K.J. Lin, and C.C. Huang) contributed equally to this work.

http://dx.doi.org/10.1016/j.biomaterials.2016.06.008
0142-9612/

been proposed as a potential strategy for enhancing the cytotoxicity of DOX. The optimal therapy schedule to maximize DOX cytotoxicity in this synergistic action involves pretreating the tumor cells with free $1,25(OH)_2D_3$ and, 24 h later, with the anticancer drug alone.

To provide localized drug delivery with the desired sequence-specific release patterns in a time-controllable manner, this work proposes an injectable, stimuli-responsive co-delivery system that is based on cationic liposomes (Lipos) that are adsorbed on anionic hollow microspheres (HMs) *via* electrostatic interaction (Lipos-HMs, Fig. 1). The cationic Lipos contain $1,25(OH)_2D_3$ and a bubble-generating agent, ammonium bicarbonate (ABC, NH_4HCO_3), and the anionic HMs are fabricated from poly(D,L-lactic-co-glycolic acid) (PLGA). The polymer shell and the aqueous core of each HM contain iron oxide nanoparticles (IONPs) and DOX, respectively. The IONPs that are doped into the PLGA shell can generate heat in response to a non-contact stimulus in a high-frequency magnetic field (HFMF).

Fig. 1 presents the mechanism of localized sequence-specific drug release by the proposed Lipos-HMs system based on the reported optimal schedule [11,14,15]. Upon heating to a temperature of around 41 °C for 10 min by exposure to HFMF, the ABC that is encapsulated in the Lipos rapidly decomposes to form CO_2 bubbles, producing permeable defects in their lipid bilayers, inducing a rapid release of $1,25(OH)_2D_3$ (first-step release), and subsequently generating a high local drug concentration extracellularly. After diffusing into cells, $1,25(OH)_2D_3$ considerably reduces the cytoplasmic level of the antioxidant enzyme SOD, reducing the capacity of the cells to withstand assault by the ROS-generating DOX. When the local temperature exceeds the glass transition temperature (T_g) of PLGA (*ca.* 40 °C), the mobility of the polymer chains is increased, greatly enlarging local voids and thereby releasing DOX from the HMs. Therefore, the entangled PLGA molecules in the HM shell may function as a "molecular switch" that controls drug release. As the heating duration is relatively short (10 min), the extent of release of DOX from the HMs is relatively low.

Twenty-four hours later, the Lipos-HMs are exposed for a longer time (45 min) to HFMF, so the PLGA "molecular switch" in the shells of the HMs is activated for a longer period, greatly increasing the amount of DOX released (second-step release). The ROS-mediated cytotoxicity is therefore enhanced by a reduced level of SOD and a locally high concentration of DOX. Co-delivery of a chemopreventive agent and an antitumor drug in a single carrier system, which can provide on-demand sequence-specific release profiles, not only improves patients' compliance with medication regimens by reducing the frequency of injections, but can also achieves synergistic effects that promote the inhibition of tumor growth. The proposed Lipos-HMs system may be applied to solid tumors with well-defined localization *via* local or endoscopic injection.

2. Materials and methods

2.1. Materials

Poly(vinyl alcohol) (PVA, MW 30–70 kDa), PLGA (with a lactide:glycolide molar ratio of 50:50, MW 24–38 kDa), and $1,25(OH)_2D_3$ were purchased from Sigma-Aldrich (St. Louis, MO, USA), while DOX was obtained from Fisher Scientific (Waltham, MA, USA). Dipalmitoylphosphatidylcholine (DPPC), cholesterol, distearoylphosphatidylethanolamine-polyethylene glycol 2000 (DSPE-PEG2000), and 1,2-di-*O*-octadecenyl-3-trimethylammonium propane (DOTMA) were acquired from Avanti Polar Lipids (Alabaster, AL, USA). All other chemicals and reagents were of analytical grade.

2.2. Preparation and characterization of Lipos-HMs

Lipid film hydration was used to prepare the test Lipos [16,17]. Briefly, a mixture of DPPC, cholesterol, DSPE-PEG2000, and DOTMA at a molar ratio of 60:40:5:5 was dissolved in chloroform. The organic solvent was removed using a rotavapor under reduced pressure until a thin lipid film was formed. This lipid film was hydrated using an aqueous solution that contained ABC (2.7 M) and $1,25(OH)_2D_3$ (0.1 μM). The mixture was then sonicated, before undergoing sequential extrusions at room temperature to control the

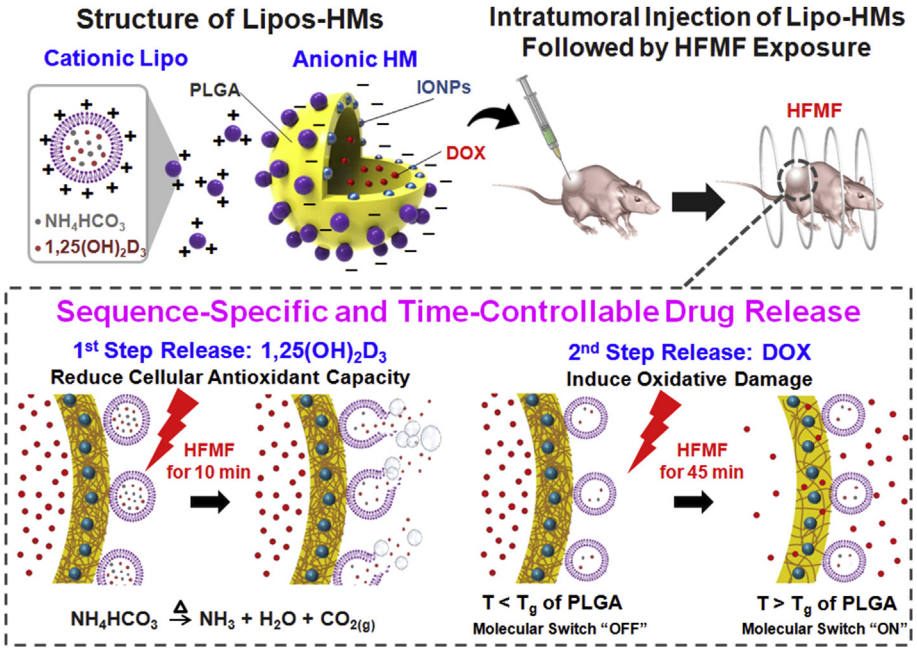

Fig. 1. Structure of Lipos-HMs developed herein and mechanism of their localized sequential release of a chemopreventive agent ($1,25(OH)_2D_3$) and an anticancer drug (DOX) in a time-controllable manner upon application of an external high-frequency magnetic field (HFMF) to enhance therapeutic effectiveness in cancer treatment. Lipos: liposomes; HMs: PLGA hollow microspheres; DOX: doxorubicin.

size of the obtained Lipos. The free ABC and $1,25(OH)_2D_3$ were removed by dialysis against an aqueous solution that contained 5 mM NaCl and 10 wt% sucrose.

IONPs were prepared by dissolving $FeCl_2 \cdot 4H_2O$ and $FeCl_3 \cdot 6H_2O$ (1:2 in molar ratio) in deionized (DI) water, to which an aqueous solution of NaOH (1.0 M) was then added to cause precipitation. Thirty minutes later, oleic acid (with a 2:1 molar ratio of oleic acid to IONPs) was added as a stabilizer [18]. The obtained IONPs were then thoroughly rinsed by acetone to remove the free oleic acid. HMs of PLGA (10 mg/mL) that contained IONPs (6 mg/mL) and DOX (1 mg/mL) were prepared using a water-in-oil-in-water (W/O/W) double-emulsion, solvent-diffusion-evaporation technique, which has been described previously [19,20]. The T_g of PLGA HMs was evaluated using a differential scanning calorimeter (DSC, Perkin-Elmer, Norwalk, CT, USA); the heating rate was controlled at 10 °C/min, and each sample was heated and cooled for five cycles between 20 and 60 °C.

To prepare Lipos-HMs, a Lipo colloidal suspension (5 mg) was added dropwise into an aqueous solution of PLGA MHs (2 mg) with magnetic stirring. The obtained particles (Lipos-HMs) in the mixed solution were then collected by centrifugation. To demonstrate the adsorption of Lipos on the surface of HMs, the Lipos were labeled with DiD (with far-red lipophilic fluorescence), while the PLGA shells of the HMs were doped with DiO (a green lipophilic dye). The as-prepared Lipos-HMs were then observed under a confocal laser scanning microscope (CLSM, TCS SL, Leica, Germany).

The zeta potentials of the Lipos, PLGA HMs, and Lipos-HMs were measured by dynamic light scattering (DLS, Zetasizer, 3000HS, Malvern Instruments Ltd., Worcestershire, UK), and their morphologies and sizes as well as characteristic energy dispersive X-ray (EDX) spectra were observed by scanning electron microscopy (SEM, JEOL JSM-5600, Tokyo, Japan). The ultrastructure of the Lipos-HMs was further investigated by transmission electron microscopy (TEM, JEOL 2010F, JEOL); the test samples were embedded in Tissue-Tek OCT compound (Sakura Finetek, Tokyo, Japan), snap-frozen in liquid N_2, and sectioned into slices with a thickness of 3 μm. To directly showing the Lipos that were adsorbed on the surface of HMs, the as-prepared Lipos-HMs were fixed with osmium tetroxide prior to observation by TEM. The heating capacity of Lipos-HMs was evaluated from the area of their hysteresis loop that was obtained using a vibrating sample magnetometer (VSM, Lake Shore Cryotronics, Westerville, Ohio, USA) at 300 K in a ±15 kOe applied magnetic field. The drug loading efficiency and content were calculated using the equations shown below.

$$\text{Loading efficiency(wt\%)} = \frac{\text{amount of drug in particles}}{\text{total amount of drug added}} \times 100\%$$

$$\text{Loading content(wt\%)} = \frac{\text{amount of drug in particles}}{\text{weight of particles}} \times 100\%$$

In the stability study, Lipos-HMs were incubated in phosphate-buffered saline (PBS) at 4 °C for two months. The stability of Lipos-HMs was determined by analyzing their zeta potential *via* DLS and examining their morphology using a fluorescence microscope.

2.3. Heating effects and sequence-specific release patterns of Lipos-HMs

The heating effects and sequence-specific release patterns of the Lipos-HMs in 5 ml of PBS (0.5 mg/mL) were characterized by applying an alternative magnetic field of 50–100 kHz and 15 kW. The bulk temperature of the test media was measured using an alcohol thermometer, while the generation of CO_2 bubbles was observed using an ultrasound imaging system (Z-one, Zonare; Mountain View, CA, USA). The amounts of $1,25(OH)_2D_3$ and DOX that were released from the test Lipos-HMs were obtained by ELISA (EIAab Science, Wuhan, China) and fluorescence spectrometry (Ex/Em. 470/585 nm, Spex FluoroMax-3, Horiba JobinYvon, Edison, NJ, USA), respectively.

2.4. Reduction of intracellular SOD expression

The reduction of the intracellular expression of SOD in human breast cancer MCF-7 cells (ATCC® HTB-22) by $1,25(OH)_2D_3$ that was released from Lipos-HMs in response to the stimulus of HFMF for 10 min was assessed. In the study, MCF-7 cells were incubated onto 35 mm ibidi μ-dish (ibidi GmbH, Munich, Germany) at a density of 1×10^5 cells/dish in Eagle's Minimum Essential Medium supplemented with 10% fetal bovine serum. After incubation for predetermined time intervals, cells were fixed with 4% paraformaldehyde and then intracellularly stained with mouse anti-human SOD and Alexa Fluor 488 conjugated goat anti-mouse antibodies (Abcam, Cambridge, MA, USA). The expression of SOD in cells was then qualitatively assessed using a CLSM and quantitatively determined by a flow cytometer (Beckman Coulter, CA, USA).

2.5. Cell viability assay

$1,25(OH)_2D_3$ can greatly reduce the intracellular expression of SOD, increasing the ROS-dependent cytotoxicity of DOX [21]. MCF-7 cells were seeded onto 35 mm ibidi μ-dish at a density of 1×10^5 cells/dish. Following treatment with Lipos-HMs and exposure to HFMF (for 10 min on day 0 and then 45 min on day 1), cells were stained with 2′,7′-dichlorofluorescin diacetate (DCFH-DA, Invitrogen, Carlsbad, CA, USA), which is a non-fluorescence probe that can be deacetylated by intracellular esterases to DCFH, which can then be oxidized to highly fluorescent DCF by ROS [22]. Accumulations of DOX and ROS in the treated cells were thus analyzed by CLSM and flow cytometry. The effect of Lipos-HMs on cell viability at 48 h following stimulation by HFMF was investigated. MCF-7 cells were seeded onto 96-well microplates at a density of 5×10^4 cells/well. The viability of the test cells was qualitatively assessed by calcein acetoxymethyl ester (calcein-AM, Invitrogen) staining and quantitatively determined using the 3-(4,5-dimethylthiazol-2-yl)-2,5-diphenyltetrazolium bromide (MTT) assay. In the MTT assay, the cells were incubated in a medium that contained 1 mg/mL MTT (Sigma-Aldrich) at 37 °C for 4 h. The metabolized MTT was then dissolved in dimethyl sulfoxide, and its absorbance was obtained in a multi-mode microplate reader (SpectraMax M5, Molecular Devices, Sunnyvale, CA, USA).

2.6. In vivo efficacy

Female nude mice (BALB/cAnN.Cg-Foxn1nu/CrtlNarl, six to eight weeks old) were purchased from the National Laboratory Animal Center, Taiwan. Animals were cared for and used according to the "Guide for the Care and Use of Laboratory Animals", which was written by the Institute of Laboratory Animal Resources, National Research Council, and published by the National Academy Press in 1996. The Institutional Animal Care and Use Committee of National Tsing Hua University approved the protocol.

To study the release of the drug from the test Lipos-HMs that were implanted subcutaneously, mice were exposed to HFMF at 50–100 kHz and 15 kW (n = 3). Fluorescence images of DOX before and after exposure to HFMF were acquired using an *in vivo* imaging system (IVIS, Xenogen, Alameda, CA, USA). The fluorescence intensities (p/sec/cm^2/sr) were determined using Living Image

software, and the local temperature was measured by an infrared (IR) thermal camera (ICI7320, Infrared Camera Inc., Beaumont, TX, USA) immediately after the animals were removed from HFMF. Free DOX was used as a control (n = 3).

To evaluate the antitumor efficacy, the MCF-7 cells were implanted subcutaneously (1×10^7 cells in 100 μL of Matrigel, BD Biosciences, San Jose, CA, USA) in the right flank region of the mice. When the tumor volumes reached 150–200 mm^3, the mice were divided into five groups. The mice in each group (n = 5) were treated under one of the following test conditions *via* the intratumoral injection; PBS (untreated control), free $1,25(OH)_2D_3$, free DOX, free $1,25(OH)_2D_3$ + free DOX, and Lipos-HMs. All animals received the same doses of $1,25(OH)_2D_3$ (4 μg/kg) and DOX (10 mg/kg); the combination dosage used was based on previous reports [11–13]. This process was repeated every four days for a total of four treatment sessions. The size of each tumor was measured using a pair of caliper, and the tumor volume was estimated as length × width × height × π/6. The tumor volumes and body weights of the test mice were measured every other day and normalized to their initial values [23,24].

At the end of repeated treatments, the mice fasted overnight were anesthetized with isoflurane (2% in 100% O_2) and injected with 0.32 mCi ^{18}F-flourodeoxyglucose (^{18}F-FDG) in 100 μL of saline *via* the tail vein. One hour after ^{18}F-FDG injection, a positron emission tomographic (PET) scanner (Inveon™, Siemens Medical Solutions, Knoxville, TN, USA) was used to acquire an image over 10 min. Following PET scanning, whole-body computed tomography (CT) images were obtained using NanoSPECT/CT (Bioscan, Washington, DC, USA). Finally, the mice were photographed and then sacrificed, and the tumor tissues were retrieved and fixed in 10% neutral buffered formalin, embedded in paraffin, sectioned, and stained with hematoxylin–eosin (H&E). TUNEL (terminal deoxynucleotidyl transferase dUTP nick end labeling) assays were carried out using an *in situ* cell death detection kit (Roche Diagnostics GmbH, Mannheim, Germany).

2.7. Statistical analysis

All results are presented as mean ± standard deviation. The two-tailed Student *t*-test was utilized to compare the means of two groups. One-way analysis of variation (ANOVA) was followed by the Bonferroni post hoc test to assess variations among three or more groups. Differences were regarded as significant at $P < 0.05$.

3. Results and discussion

Combination chemotherapy has attracted considerable interest recently for the treatment of various cancers [25,26]. As an example, the use of a chemopreventive agent $1,25(OH)_2D_3$ has been proposed to enhance the cytotoxic activity of ROS-generating compounds, such as DOX [11,27]. However, the probability that these drug molecules reach the diseased tissues at the proper time and effective therapeutic concentrations is very low, limiting the efficacy of their synergistic activities. To overcome these difficulties, this work develops an injectable, stimuli-responsive co-delivery system of Lipos-HMs that can release $1,25(OH)_2D_3$ and DOX in a specific sequence and a time-controllable manner, concentrating the drug in tumor tissues. The experimental results demonstrate that this combination drug-delivery system for the sequential actions of $1,25(OH)_2D_3$ and DOX greatly improves the cytotoxicity of DOX, increasing therapeutic outcome.

3.1. Characteristics of Lipos-HMs

In this work, the lipid film hydration technique, followed by sequential extrusion, was utilized to prepare Lipos that contained $1,25(OH)_2D_3$ and ABC. DLS measurements indicate that the zeta potential of the as-prepared Lipos was 17.0 ± 3.7 mV (n = 6 batches, Fig. 2a). The as-prepared Lipos were spherical particles with diameters from 120 to 150 nm. The loading efficiency of $1,25(OH)_2D_3$ in the Lipos was 14.1 ± 4.2% (n = 6 batches).

The magnetically responsive PLGA HMs, whose polymer shells were doped with IONPs and aqueous cores contained DOX, were fabricated using a W/O/W double-emulsion method. The as-fabricated PLGA HMs had a negative zeta potential of −18.1 ± 2.1 mV (Fig. 2a) and a DOX loading efficiency of 21.6 ± 6.8% (n = 6 batches).

The Lipos-HMs were then prepared by mixing a suspension of Lipos with an aqueous solution of PLGA HMs. When the cationic Lipos were in contact with the anionic PLGA HMs, electrostatic attractions caused Lipos to be adsorbed on the surface of each HM, switching the negative zeta-potential of the HMs to positive (3.6 ± 1.7 mV, Fig. 2a). As observed by SEM, the Lipos-HMs retained their spherical morphologies with diameters from 2 to 3 μm (Fig. 2b); their characteristic EDX spectrum confirmed that they contained Fe (IONPs, Fig. 2c). The TEM image in Fig. 2d revealed a hollow structure of each Lipos-HM, with a uniform shell thickness of around 250 nm; additionally, the IONPs were uniformly distributed in their PLGA shells with diameters of 10–12 nm, and test Lipos were tightly adsorbed on the surface of each HM *via* electrostatic interaction (Fig. 2e).

The adsorption of Lipos on HMs was further demonstrated using CLSM. According to Fig. 2f, the PLGA shells of the HMs that were doped with DiO were green, while their aqueous cores of DOX were red. When the DiD-labeled Lipos (purple color) were adsorbed on the outer shells of the HMs, the particles became purple. These experimental data suggest that cationic liposomes that are adsorbed on anionic hollow microspheres *via* electrostatic interaction. The loading contents of $1,25(OH)_2D_3$ and DOX in Lipos-HMs were 0.0022 ± 0.0007% and 5.6 ± 1.4%, respectively (n = 6 batches).

Particles with relatively large size (>500 nm) are hardly internalized by non-phagocytic cells [28–31]. Therefore, it is expected that the as-prepared Lipos-HMs be localized extracellularly after intratumoral injection.

In the stability study, the as-prepared Lipos-HMs were stored in PBS for two months. The zeta potential of Lipos-HMs remained approximately constant throughout the study (3.8 ± 2.0 mV; $P > 0.05$), and no aggregation or precipitation of the test particles was observed, most likely because of the electrostatic repulsion between the positively charged Lipos-HMs. Fluorescence images verify that the Lipos remained stably adsorbed on the surface of HMs (Fig. 2f).

3.2. Effects of heating on Lipos-HMs and their sequence-specific drug release patterns

In an externally applied HFMF, magnetic materials such as IONPs are heated owing to hysteresis losses, which can be estimated from the area of their hysteresis loop, which can be determined using a VSM [32]. The area of the loop is proportional to the specific absorption rate, which is defined as the heating power of a magnetic sample per gram [33,34]. According to Fig. 3a, both free IONPs and Lipos-HMs exhibited hysteresis loops upon exposure to HFMF, revealing their potential to generate heat, suggesting that magnetism of IONPs was preserved after the formation of the Lipos-HMs. However, encapsulation of IONPs in Lipos-HMs greatly reduced the heating power from 7.5 to 2.8 W/g, as a result of the increase in mass of the particles when PLGA and lipids were incorporated.

No significant change in temperature was observed when the empty control (PBS only) or the PBS with Lipos was exposed to

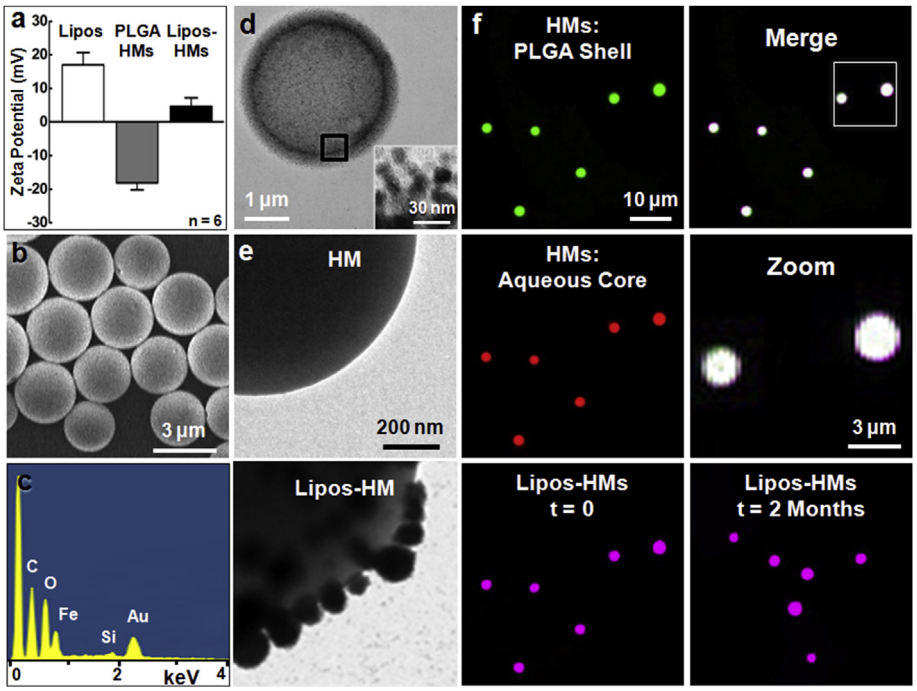

Fig. 2. (a) Zeta potential values of Lipos, PLGA HMs, and Lipos-HMs. (b) SEM micrograph of Lipos-HMs and (c) their characteristic EDX spectrum. (d) TEM micrographs that revealed hollow structure of a Lipos-HM and IONPs encapsulated in its PLGA shell. (e) TEM micrographs showing the adsorption of Lipos on a PLGA HM. (f) Fluorescence images of PLGA shells and aqueous cores of HMs, and images of Lipos-HMs before and after storage.

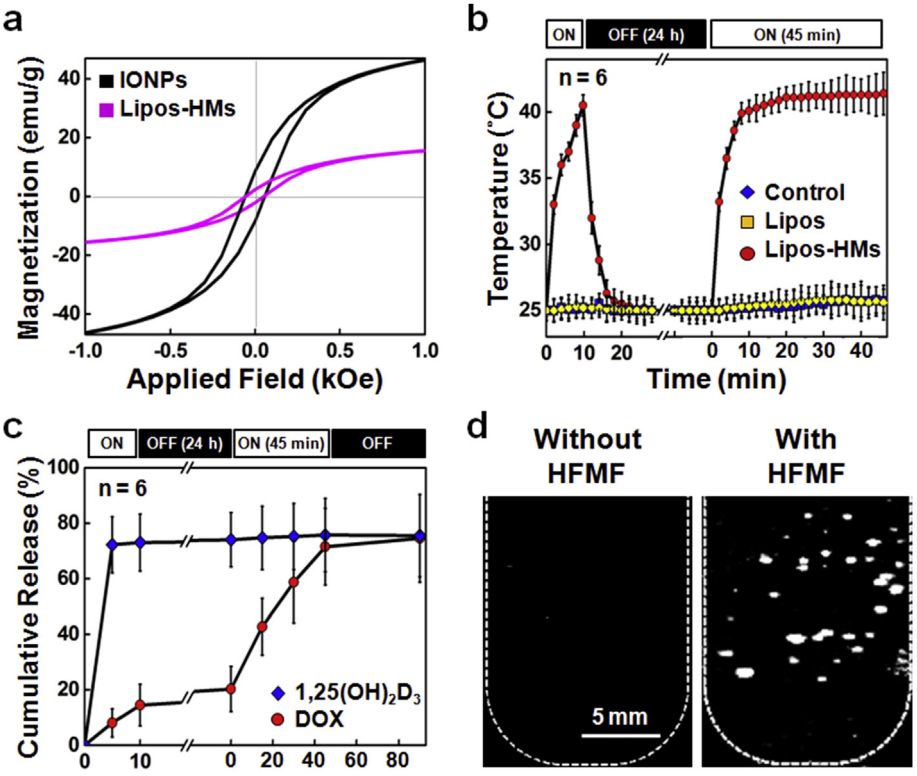

Fig. 3. (a) VSM measurements of magnetization of IONPs and Lipos-HMs. (b) Changes in local temperatures of control (PBS), Lipos, and Lipos-HMs during exposure to HFMF. (c) Release profiles of $1,25(OH)_2D_3$ and DOX from Lipos-HMs incubated in PBS under HFMF. (d) Ultrasound images of Lipos-HMs in PBS, showing generation CO_2 bubbles upon HFMF treatment. VSM: vibrating sample magnetometer.

HFMF (Fig. 3b). In contrast, upon exposure to HFMF, the temperature of the suspension of Lipos-HMs in PBS rose promptly, reaching a plateau of approximately 41 °C within 5 min (Fig. 3b). According to the relevant literature, mild hyperthermia (38–42 °C) has no cytotoxic effect on cells [35]. These experimental results show that the Lipos-HMs prepared herein could convert magnetic energy into

local heat in an external magnetic field, increasing the local temperature, including the Lipos that were adsorbed on HMs and their PLGA shell matrices.

Fig. 3c presents typical profiles of the release of $1,25(OH)_2D_3$ and DOX from suspensions of Lipos-HMs upon heating in HFMF. During a short period (10 min) of stimulation by HFMF, the local temperature rapidly increased to around 41 °C (Fig. 3b), causing the ABC that was encapsulated in the aqueous compartment of Lipos to decompose and generate CO_2 bubbles (Fig. 3d). Once their internal pressure reached a certain level, the gas bubbles permeated the membrane and formed a transient pore [36], causing the rapid release of $1,25(OH)_2D_3$ locally. About 75% of the $1,25(OH)_2D_3$ that was loaded into the Lipos was detected in the test medium within 5 min, while only 15% of the DOX was released from the PLGA HMs during this period (first-step release).

The rate of diffusion of drug molecules in a polymer matrix depends on various factors, the most important of which is the temperature of the system relative to the T_g of the polymer. As determined by DSC, the T_g of PLGA HMs was 39.8 ± 1.2 °C (n = 6). When the environmental temperature is lower than their T_g, the mobility of their polymer chains is limited so the PLGA "molecular switch" in the shells of the HMs is deactivated, such that release of the drug from the HMs is minimal. When the temperature of the system rises above T_g, the polymer mobility increases considerably and the PLGA "molecular switch" is turned on; therefore, the diffusion of the drug molecules through the HMs increases remarkably. This process is reversible.

During the 24 h of incubation after HFMF was switched off, the amounts of $1,25(OH)_2D_3$ and DOX that were released from the Lipos-HMs were minimal. During the second exposure to HFMF for 45 min, essentially no $1,25(OH)_2D_3$ released from the Lipos, whereas the rate of DOX release from the PLGA HMs increased rapidly, causing a significant increase in cumulative release of up to around 75% (second-step release). These empirical results indicate that the Lipos-HMs can act as a co-delivery platform, carrying $1,25(OH)_2D_3$ and DOX in Lipos and PLGA HMs, respectively, with the desired sequence-specific drug release patterns whose timing can be controlled.

3.3. Reduction of cytoplasmic SOD expression by $1,25(OH)_2D_3$

Studies have reported that $1,25(OH)_2D_3$ can substantially reduce the cytoplasmic expression of the antioxidant enzyme SOD, which plays a major role in cellular defense against oxidative damage [10,21]. The effect of $1,25(OH)_2D_3$ that was released from Lipos-HMs in response to stimulation by HFMF on the expression of SOD in MCF-7 tumor cells was evaluated. To prevent the generation of misleading results by the direct cytotoxicity of DOX, the Lipos-HMs that were used in this part of the work did not contain DOX. The amount of $1,25(OH)_2D_3$ that was incorporated into Lipos-HMs equaled that used in the control group, which received free $1,25(OH)_2D_3$. Following treatment, the expression levels of SOD were detected by immunofluorescence staining using anti-SOD antibodies and then examined by CLSM and flow cytometry at specified time points.

According to Fig. 4a and b, treatment with free $1,25(OH)_2D_3$ or Lipos-HMs greatly reduced the fluorescence intensity of SOD within the MCF-7 cells, suggesting a significant reduction of the intracellular expression of SOD ($P < 0.05$). The reduction in SOD level in the control group that received free $1,25(OH)_2D_3$ exceeded that in the group that was treated with Lipos-HMs, but not significantly so different ($P > 0.05$). These experimental results demonstrate that the $1,25(OH)_2D_3$ that was released from Lipos-HMs could effectively reduce the level of SOD expressed in tumor cells, potentially promoting the accumulation of ROS that was produced intracellularly following the cellular uptake of an anticancer drug (such as DOX).

3.4. Cellular uptake of DOX and intracellular accumulation of ROS

Following treatment with Lipos-HMs and exposure to HFMF, the cellular uptake of the released DOX by MCF-7 cells and their intracellular accumulation of ROS were studied; the results were compared with those obtained using free DOX. As presented in Fig. 5a, DOX primarily accumulated in the nuclei of the treated cells. The cells that received Lipos-HMs had a lower fluorescence intensity than those treated with free DOX (70.3 ± 0.6%, n = 6,

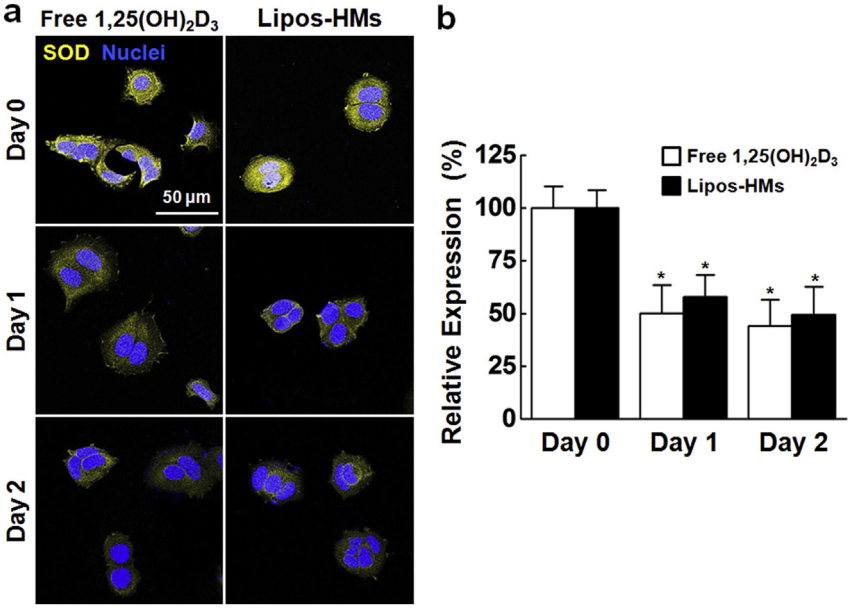

Fig. 4. (a) CLSM immunofluorescence images and (b) expression levels of SOD in MCF-7 tumor cells that were incubated with free $1,25(OH)_2D_3$ or Lipos-HMs for various periods, determined by flow cytometry. SOD: superoxide dismutase. *$P < 0.05$ *vs.* same group at day 0.

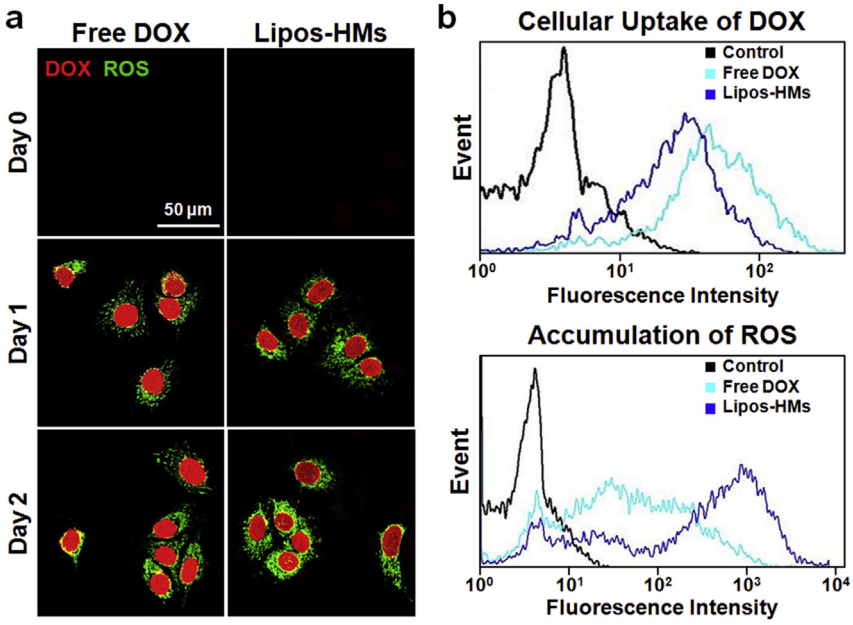

Fig. 5. (a) CLSM fluorescence images and (b) flow cytometry histograms of cellular uptake of DOX and intracellular accumulation of ROS in MCF-7 tumor cells that were incubated with free DOX or Lipos-HMs, obtained at indicated time points.

$P < 0.05$, Fig. 5b), suggesting the cellular uptake of DOX in the former group was less than in the latter group. This result is likely because only approximately 75% of the DOX was released from Lipos-HMs following exposure to HFMF (Fig. 3c).

Upon cellular uptake, DOX induces the production of ROS [7,37]. DCFH-DA staining provided visible evidence of ROS accumulation in MCF-7 cancer cells that were treated with free DOX or Lipos-HMs. On day two of incubation, the ROS fluorescent signal that was obtained from the cells that were incubated with Lipos-HMs appeared to be 2.2-fold stronger (221.0 ± 37.1%, n = 6) than that obtained from those that were incubated with free DOX ($P < 0.05$). These analytical data reveal that Lipos-HMs remarkably enhanced the accumulation of ROS in tumor cells because $1,25(OH)_2D_3$ reduced their cytoplasmic SOD expression, despite the lower cellular uptake of DOX. The excess intracellularly accumulated ROS may oxidize and damage membrane lipids, proteins, polysaccharides, and DNA, resulting ultimately in cell death [9,38].

3.5. Synergistic effects on cell viability

The effect of $1,25(OH)_2D_3$-potentiated DOX-induced toxicity on the viability of MCF-7 cells following treatment with Lipos-HMs upon exposure to HFMF was evaluated using calcein-AM staining and the MTT assay. In calcein-AM staining, live cells appear green. The untreated cells (untreated control) and those treated with empty Lipos-HMs (that contained no $1,25(OH)_2D_3$ and DOX, but

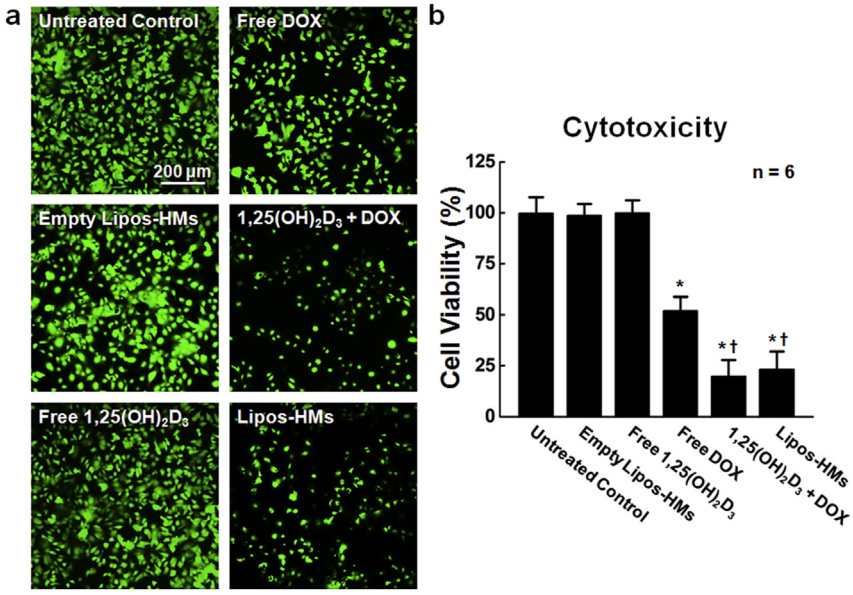

Fig. 6. (a) CLSM images of live cells stained by Calcein-AM and (b) results of MTT assay of MCF-7 cells following various treatments. *$P < 0.05$ *vs.* untreated control; †$P < 0.05$ *vs.* free DOX.

were exposed to HFMF with a hyperthermic temperature of 41 °C), free $1,25(OH)_2D_3$, free DOX, or free $1,25(OH)_2D_3$ + free DOX were used as controls. The concentrations of free $1,25(OH)_2D_3$ (10 nM) and free DOX (10 μg/mL) were equivalent to those that were incorporated into the Lipos-HMs.

A comparison with the untreated control group (Fig. 6a and b) revealed no cytotoxicity in the cells that were treated with empty Lipos-HMs or free $1,25(OH)_2D_3$ alone ($P > 0.05$; ANOVA + Bonferroni test). The MCF-7 cells that were treated with a combination of free $1,25(OH)_2D_3$ + free DOX or Lipos-HMs had greater cytotoxicity than those that received free DOX alone. Free DOX yielded a 52 ± 6.7% cell viability, while free $1,25(OH)_2D_3$ + free DOX and Lipos-HMs resulted in significantly lower cell viabilities of 19.8 ± 8.0% and 23.1 ± 8.9%, respectively ($P < 0.05$, ANOVA + Bonferroni test). Hence, treatment with $1,25(OH)_2D_3$ significantly exacerbated the damage that was caused by DOX in MCF-7 cells, exhibiting synergistic cytotoxic effects. These findings indicate that Lipos-HMs considerably enhanced the intracellular accumulation of ROS by reducing SOD expression, increasing the susceptibility of cancer cells to the cytotoxic action of the commonly used anticancer drug, DOX.

3.6. *In vivo* release of drug molecules

The *in vivo* release of drug molecules, which was obtained from the biodistribution of their fluorescence images, from the test Lipos-HMs was demonstrated and monitored using an IVIS; however, only the fluorescence of DOX was detectable because $1,25(OH)_2D_3$ does not fluoresce. To gain insight into the *in vivo* release of DOX, mice were subcutaneously treated with Lipos-HMs by direct local injection; the mice that were treated with free DOX served as a control. A significant decrease in its fluorescence intensity was detected within 1 h of the injection of free DOX (with a 65.0 ± 13.0 decrease, n = 3, Fig. 7a), suggesting that the drug was

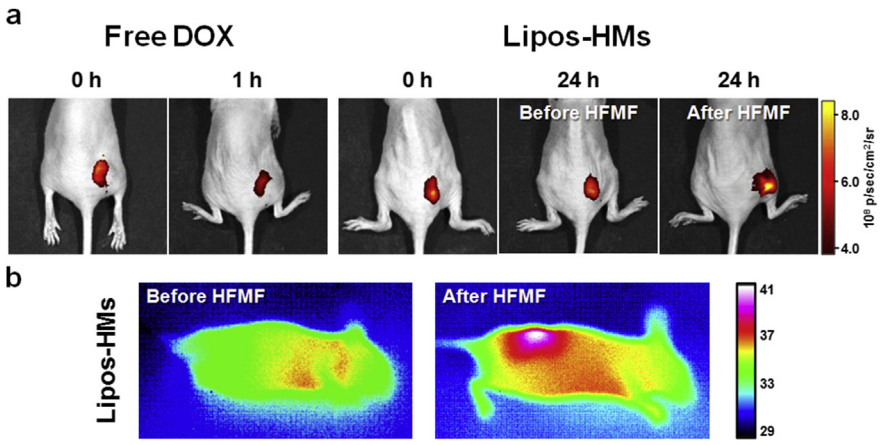

Fig. 7. (a) *In vivo* biodistribution obtained from DOX fluorescence images captured using an *in vivo* imaging system (IVIS) and (b) thermographic images of mice following direct local injection of free drug or Lipos-HMs under exposure to HFMF.

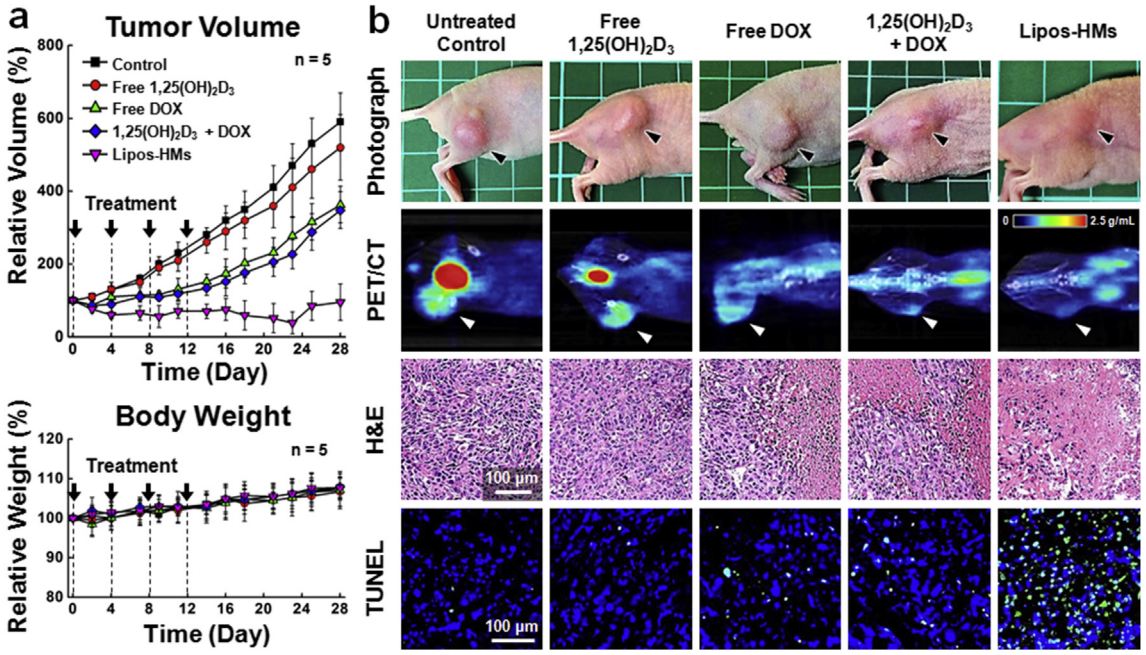

Fig. 8. (a) Changes in relative tumor volume and body weight and (b) photographs, ^{18}F-FDG PET/CT co-registered images, and histological photomicrographs of tumor sections stained with H&E or TUNEL of mice that received various treatments.

rapidly lost at the site of injection, limiting its therapeutic efficacy.

At high concentrations of DOX within HMs, the fluorescence signal of DOX is quenched; upon release through the shells, its fluorescence intensity increases significantly [39,40]. In the absence of a stimulus by HFMF, the local fluorescence intensity of DOX in the skin that received Lipos-HMs remained constant for a period of 24 h, suggesting that the diffusion of DOX through the PLGA shells of the HMs was rather slow. Upon exposure to HFMF, the local temperature increased rapidly to around 41 °C (Fig. 7b), and the skin exhibited a fluorescence intensity of DOX that was 3.3 times that in the absence of HFMF (with a 333.8 ± 55.0% enhancement, n = 3), revealing that the Lipos-HMs were stimulated to release rapidly their encapsulated drug in their neighborhood. These analytical data indicate that Lipos-HMs eluted a negligible concentration of DOX without the HFMF stimulus, but that most of their released drug was concentrated locally when exposed to HFMF. These data suggest that spatial fixation of free drugs can be achieved by encapsulation of free drugs into a drug delivery system. No significant skin damage was observed following the HFMF treatment.

3.7. Synergistic effects of Lipos-HMs on antitumor efficacy

The synergistic effects of intratumorally injected Lipos-HMs on the antitumor efficacy were examined in nude mice that bore MCF-7 xenograft tumors. A comparison with the untreated control revealed that treatment with free 1,25$(OH)_2D_3$ did not significantly affect the suppression of tumor growth ($P > 0.05$, Fig. 8a). Improved antitumor activity was observed in the groups that received free DOX or free 1,25$(OH)_2D_3$ + free DOX ($P < 0.05$); however, their tumor growth progressed with time, likely because of the rapid clearance of free drugs from the injection site. In marked contrast, the group that was treated with Lipos-HMs and was exposed to HFMF exhibited the effective inhibition of tumor growth throughout the study ($P < 0.05$). The body weight of the tumor-bearing mice increased slightly throughout the period of investigation, reflecting no general toxicity of treatment with Lipos-HMs.

At the end of treatment, the antitumor efficacy of therapeutic intervention of Lipos-HMs was further examined by a PET scanner, with ^{18}F-FDG as an imaging probe, revealing the metabolic (or proliferative) activity of tumor tissues [41]. According to Fig. 8b, the tumor metabolic activity in the mice that were treated with Lipos-HMs under exposure to HFMF was substantially lower than that in those in the control groups that underwent no treatment, or were treated with free 1,25$(OH)_2D_3$, free DOX, or free 1,25$(OH)_2D_3$ + free DOX.

H&E staining and TUNEL assay were also performed to explore the death of tumor cells. Animals that received no treatment or free 1,25$(OH)_2D_3$ exhibited no evidence of cell destruction. In contrast, significant cell death was identified in the groups that had been treated with free DOX or free 1,25$(OH)_2D_3$ + free DOX, and considerably more apoptotic tumor cells were detected in the group that had received Lipos-HMs. The above empirical data indicate that the sequential releases of 1,25$(OH)_2D_3$ and DOX from Lipos-HMs based on their optimal therapy schedule was the most effective therapeutic intervention of all of those investigated. However, an orthotopic tumor model may be required for further validating the clinical relevance of the proposed carrier system.

4. Conclusions

This work developed a Lipos-HMs co-delivery system that allowed active molecules of 1,25$(OH)_2D_3$ and DOX to be released within a tumor in a sequence-specific and time-controllable manner using a remotely regulated magnetic field. Experimental results reveal that the sequential release of 1,25$(OH)_2D_3$ and DOX from the Lipos-HMs significantly reduced the cytoplasmic expression of SOD, enhanced the intracellular accumulation of ROS, and increased DOX-induced toxicity, maximizing the inhibition of tumor growth. The synergistic delivery of a chemopreventive agent and an anticancer drug with complementary actions by the same carrier system is a promising strategy for improving the therapeutic efficacy of chemotherapy.

Acknowledgments

The authors would like to thank the Ministry of Science and Technology of Taiwan (ROC) for financially supporting this research (Contract No. MOST 104-2314-B-007-001 -MY3).

References

[1] D. Peer, J.M. Karp, S. Hong, O.C. Farokhzad, R. Margalit, R. Langer, Nanocarriers as an emerging platform for cancer therapy, Nat. Nanotechnol. 2 (2007) 751–760.
[2] L.H. Hurley, DNA and its associated processes as targets for cancer therapy, Nat. Rev. Cancer 2 (2002) 188–200.
[3] E. Senkus, S. Kyriakides, S. Ohno, F. Penault-Llorca, P. Poortmans, E. Rutgers, et al., Primary breast cancer: ESMO Clinical Practice Guidelines for diagnosis, treatment and follow-up, Ann. Oncol. 26 (Suppl 5) (2015) v8–30.
[4] R.V. Chari, Targeted cancer therapy: conferring specificity to cytotoxic drugs, Acc. Chem. Res. 41 (2008) 98–107.
[5] J. Panyam, V. Labhasetwar, Biodegradable nanoparticles for drug and gene delivery to cells and tissue, Adv. Drug Deliv. Rev. 55 (2003) 329–347.
[6] Y. Malam, M. Loizidou, A.M. Seifalian, Liposomes and nanoparticles: nanosized vehicles for drug delivery in cancer, Trends Pharmacol. Sci. 30 (2009) 592–599.
[7] H.G. Keizer, H.M. Pinedo, G.J. Schuurhuis, H. Joenje, Doxorubicin (adriamycin): a critical review of free radical-dependent mechanisms of cytotoxicity, Pharmacol. Ther. 47 (1990) 219–231.
[8] E. Agostinelli, N. Seiler, Non-irradiation-derived reactive oxygen species (ROS) and cancer: therapeutic implications, Amino Acids 31 (2006) 341–355.
[9] V. Nogueira, N. Hay, Molecular pathways: reactive oxygen species homeostasis in cancer cells and implications for cancer therapy, Clin. Cancer Res. 19 (2013) 4309–4314.
[10] L.W. Oberley, G.R. Buettner, Role of superoxide dismutase in cancer: a review, Cancer Res. 39 (1979) 1141–1149.
[11] A. Ravid, D. Rocker, A. Machlenkin, C. Rotem, A. Hochman, G. Kessler-Icekson, et al., 1,25-dihydroxyvitamin D_3 enhances the susceptibility of breast cancer cells to doxorubicin-induced oxidative damage, Cancer Res. 59 (1999) 862–867.
[12] R. Koren, D. Rocker, O. Kotestiano, U.A. Liberman, A. Ravid, Synergistic anticancer activity of 1,25-dihydroxyvitamin D(3) and immune cytokines: the involvement of reactive oxygen species, J. Steroid Biochem. Mol. Biol. 73 (2000) 105–112.
[13] Y.L. Cho, C. Christensen, D.E. Saunders, W.D. Lawrence, G. Deppe, V.K. Malviya, et al., Combined effects of 1,25-dihydroxyvitamin D_3 and platinum drugs on the growth of MCF-7 cells, Cancer Res. 51 (1991) 2848–2853.
[14] Y. Ma, W.D. Yu, D.L. Trump, C.S. Johnson, 1,25D_3 enhances antitumor activity of gemcitabine and cisplatin in human bladder cancer models, Cancer 116 (2010) 3294–3303.
[15] R. Petrioli, A. Pascucci, E. Francini, S. Marsili, A. Sciandivasci, G. De Rubertis, et al., Weekly high-dose calcitriol and docetaxel in patients with metastatic hormone-refractory prostate cancer previously exposed to docetaxel, BJU Int. 100 (2007) 775–779.
[16] S. Koudelka, J. Turanek, Liposomal paclitaxel formulations, J. Control Release 163 (2012) 322–334.
[17] Z.X. Liao, E.Y. Chuang, C.C. Lin, Y.C. Ho, K.J. Lin, P.Y. Cheng, et al., An AS1411 aptamer-conjugated liposomal system containing a bubble-generating agent for tumor-specific chemotherapy that overcomes multidrug resistance, J. Control Release 208 (2015) 42–51.
[18] S. Sun, H. Zeng, Size-controlled synthesis of magnetite nanoparticles, J. Am. Chem. Soc. 124 (2002) 8204–8205.
[19] C.J. Ke, Y.J. Lin, Y.C. Hu, W.L. Chiang, K.J. Chen, W.C. Yang, et al., Multidrug release based on microneedle arrays filled with pH-responsive PLGA hollow microspheres, Biomaterials 33 (2012) 5156–5165.
[20] W.L. Chiang, C.J. Ke, Z.X. Liao, S.Y. Chen, F.R. Chen, C.Y. Tsai, et al., Pulsatile drug release from PLGA hollow microspheres by controlling the permeability of their walls with a magnetic field, Small 8 (2012) 3584–3588.
[21] Y. Ma, D.L. Trump, C.S. Johnson, Vitamin D in combination cancer treatment, J. Cancer 1 (2010) 101–107.
[22] C. Rota, C.F. Chignell, R.P. Mason, Evidence for free radical formation during the oxidation of 2'-7'-dichlorofluorescin to the fluorescent dye 2'-7'-dichlorofluorescein by horseradish peroxidase: possible implications for oxidative stress measurements, Free Radic. Biol. Med. 27 (1999) 873–881.

[23] Y.M. Kim, S.C. Song, Targetable micelleplex hydrogel for long-term, effective, and systemic siRNA delivery, Biomaterials 35 (2014) 7970–7977.
[24] M.F. Chung, H.Y. Liu, K.J. Lin, W.T. Chia, H.W. Sung, A pH-responsive carrier system that generates no bubbles to trigger drug release and reverse P-glycoprotein-mediated multidrug resistance, Angew. Chem. Int. Ed. Engl. 54 (2015) 9890–9893.
[25] Early Breast Cancer Trialists' Collaborative G, R. Peto, C. Davies, J. Godwin, R. Gray, H.C. Pan, et al., Comparisons between different polychemotherapy regimens for early breast cancer: meta-analyses of long-term outcome among 100,000 women in 123 randomised trials, Lancet 379 (2012) 432–444.
[26] A.Z. Wang, R. Langer, O.C. Farokhzad, Nanoparticle delivery of cancer drugs, Annu. Rev. Med. 63 (2012) 185–198.
[27] N. Lopes, J. Paredes, J.L. Costa, B. Ylstra, F. Schmitt, Vitamin D and the mammary gland: a review on its role in normal development and breast cancer, Breast Cancer Res. 14 (2012) 211.
[28] S.D. Conner, S.L. Schmid, Regulated portals of entry into the cell, Nature 422 (2003) 37–44.
[29] J. Rejman, V. Oberle, I.S. Zuhorn, D. Hoekstra, Size-dependent internalization of particles via the pathways of clathrin- and caveolae-mediated endocytosis, Biochem. J. 377 (2004) 159–169.
[30] S. Mitragotri, J. Lahann, Physical approaches to biomaterial design, Nat. Mater 8 (2009) 15–23.
[31] C. He, Y. Hu, L. Yin, C. Tang, C. Yin, Effects of particle size and surface charge on cellular uptake and biodistribution of polymeric nanoparticles, Biomaterials 31 (2010) 3657–3666.
[32] M. Ma, Y. Wu, H. Zhou, Y.K. Sun, Y. Zhang, N. Gu, Size dependence of specific power absorption of Fe_3O_4 particles in AC magnetic field, J. Magn. Magn. Mater 268 (2004) 33–39.
[33] I. Baker, Q. Zeng, W.D. Li, C.R. Sullivan, Heat deposition in iron oxide and iron nanoparticles for localized hyperthermia, J. Appl. Phys. 99 (2006).
[34] H. Kobayashi, A. Hirukawa, A. Tomitaka, T. Yamada, M. Jeun, S. Bae, et al., Self-heating property under ac magnetic field and its evaluation by ac/dc hysteresis loops of $NiFe_2O_4$ nanoparticles, J. Appl. Phys. 107 (2010).
[35] W. Rao, W. Zhang, I. Poventud-Fuentes, Y. Wang, Y. Lei, P. Agarwal, et al., Thermally responsive nanoparticle-encapsulated curcumin and its combination with mild hyperthermia for enhanced cancer cell destruction, Acta Biomater. 10 (2014) 831–842.
[36] K.J. Chen, H.F. Liang, H.L. Chen, Y. Wang, P.Y. Cheng, H.L. Liu, et al., A thermoresponsive bubble-generating liposomal system for triggering localized extracellular drug delivery, ACS Nano 7 (2013) 438–446.
[37] C. Ji, B. Yang, Y.L. Yang, S.H. He, D.S. Miao, L. He, et al., Exogenous cell-permeable C6 ceramide sensitizes multiple cancer cell lines to doxorubicin-induced apoptosis by promoting AMPK activation and mTORC1 inhibition, Oncogene 29 (2010) 6557–6568.
[38] H.U. Simon, A. Haj-Yehia, F. Levi-Schaffer, Role of reactive oxygen species (ROS) in apoptosis induction, Apoptosis 5 (2000) 415–418.
[39] R. Venkatesan, A. Pichaimani, K. Hari, P.K. Balasubramanian, J. Kulandaivel, K. Premkumar, Doxorubicin conjugated gold nanorods: a sustained drug delivery carrier for improved anticancer therapy, J. Mater Chem. B 1 (2013) 1010–1018.
[40] H.J. Lee, Y. Liu, J. Zhao, M. Zhou, R.R. Bouchard, T. Mitcham, et al., *In vitro* and *in vivo* mapping of drug release after laser ablation thermal therapy with doxorubicin-loaded hollow gold nanoshells using fluorescence and photoacoustic imaging, J. Control Release 172 (2013) 152–158.
[41] P. Habibollahi, N.S. van den Berg, D. Kuruppu, M. Loda, U. Mahmood, Metformin–an adjunct antineoplastic therapy–divergently modulates tumor metabolism and proliferation, interfering with early response prediction by ^{18}F-FDG PET imaging, J. Nucl. Med. 54 (2013) 252–258.